4676 *Chem. Mater.* **2009,** *21,* 4676–4684
DOI:10.1021/cm901789e

CHEMISTRY OF MATERIALS
Article

# Positive Constructs: Charges Localized on Surface-Confined Organometallic Oligomers

Marc Altman,[†] Olena V. Zenkina,[†] Takahiko Ichiki,[†] Mark A. Iron,[‡] Guennadi Evmenenko,[§] Pulak Dutta,[§] and Milko E. van der Boom*[,†]

[†]*Department of Organic Chemistry,* [‡]*Department of Chemical Research Support, The Weizmann Institute of Science, Rehovot, 76100, Israel, and* [§]*Department of Physics and Astronomy and the Materials Research Center, Northwestern University, Evanston, Illinois 60208-3113*

*Received June 25, 2009. Revised Manuscript Received July 23, 2009*

Assemblies with molecular-level organization based on organic chromophores and a bimetallic palladium complex are presented. A layer-by-layer strategy is employed by alternately coordinating vinylpyridine-terminated chromophores to the metal centers to form cationic oligomers. These new structures are formed from solution on quartz and silicon substrates functionalized with a covalently bound template layer. Twelve consecutive deposition steps result in structurally regular assemblies as demonstrated by linear increases in the ellipsometrically determined thickness and UV−vis optical absorption. The increase in thickness for each additional layer shows that the long-range order of the system is determined by the structure of the chromophores and by the square-planar geometry of the metal centers. Furthermore, the optical properties indicate that the conjugation length of the assembly component does not increase in the surface-bound oligomers with each additional deposition cycle. Structural communication is transferred via the system components, but they remain electronically isolated. This is supported by density functional theory (DFT) calculations.

## Introduction

The development of supramolecular chemistry has had a profound impact on the conceptualization of chemical sciences. Rather than dealing with atoms and intramolecular bonds, new structures are constructed of a diverse repertoire of molecules held together by a range of forces.[1−13] Often, metal−ligand coordination is used to enforce the structural framework. Pioneering work by Lehn has developed into a rapidly expanding field of study. In particular, a wide range of grid-type architectures based primarily on metal-ion-pyridyl interactions have been demonstrated.[14,15] In certain cases, these structures can be self-assembled at an air−water interface to produce crystalline films.[16−19] Another recent example of metal−organic supramolecular assemblies are the metallacyclic rectangles adsorbed by Stang and coworkers onto graphite and gold surfaces to form ordered structures whose orientation is governed by the nature of the complex−substrate interactions.[20] Such structures can be dynamic.[21] For instance, Nitschke and Rissanen described a tetrahedral cage based on iron coordination

*E-mail: milko.vanderboom@weizmann.ac.il.

(1) Yan, H.; Chen, Z.; Zheng, Y.; Newman, C.; Quinn, J. R.; Dotz, F.; Kastler, M.; Facchetti, A. *Nature* **2009**, *457*, 679–686.
(2) Ge, X.; Manzano, C.; Berndt, R.; Anger, L. T.; Köhler, F.; Herges, R. *J. Am. Chem. Soc.* **2009**, *131*, 6096–6098.
(3) Luo, J.; Lei, T.; Wang, L.; Ma, Y.; Cao, Y.; Wang, J.; Pei, J. *J. Am. Chem. Soc.* **2009**, *131*, 2076–2077.
(4) Kira, A.; Umeyama, T.; Matano, Y.; Yoshida, K.; Isoda, S.; Park, J. K.; Kim, D.; Imahori, H. *J. Am. Chem. Soc.* **2009**, *131*, 3198–3200.
(5) Baram, J.; Shirman, E.; Ben-Shitrit, N.; Ustinov, A.; Weissman, H.; Pinkas, I.; Wolf, S. G.; Rybtchinski, B. *J. Am. Chem. Soc.* **2008**, *130*, 14966–14967.
(6) Britt, D.; Tranchemontagne, D.; Yaghi, O. M. *Proc. Natl. Acad. Sci. U. S. A.* **2008**, *105*, 11623–11627.
(7) Skopek, K.; Hershberger, M. C.; Gladysz, J. A. *Coord. Chem. Rev.* **2007**, *251*, 1723–1733.
(8) Amijs, C. H. M.; van Klink, G. P. M.; van Koten, G. *Dalton Trans.* **2006**, 308–327.
(9) van der Boom, T.; Hayes, R. T.; Zhao, Y.; Bushard, P. J.; Weiss, E. A.; Wasielewski, M. R. *J. Am. Chem. Soc.* **2002**, *124*, 9582–9590.
(10) Reinhoudt, D. N.; Crego-Calama, M. *Science* **2002**, *295*, 2403–2407.
(11) Gade, L. H. *Angew. Chem., Int. Ed.* **2001**, *40*, 3573–3575.
(12) Cram, D. J., Cram, J. M., Eds. *Container Molecules and Their Guests*; The Royal Society of Chemisty: London, 1997.
(13) Zang, L.; Che, Y.; Moore, J. S. *Acc. Chem. Res.* **2008**, *41*, 1596–1608.
(14) Ruben, M.; Rojo, J.; Romero-Salguero, F. J.; Uppadine, L. H.; Lehn, J.-M. *Angew. Chem., Int. Ed.* **2004**, *43*, 3644–3662.
(15) Nitschke, J. R.; Lehn, J.-M. *Proc. Natl. Acad. Sci. U. S. A.* **2003**, *100*, 11970–11974.
(16) Weissbuch, I.; Baxter, P.; Cohen, S.; Cohen, H.; Kjaer, K.; Howes, P.; Als-Nielsen, J.; Hanan, G.; Schubert, U.; Lehn, J.-M.; Leiserowitz, L.; Lahav, M. *J. Am. Chem. Soc.* **1998**, *120*, 4850–4860.
(17) Weissbuch, I.; Baxter, P. N. W.; Kuzmenko, I.; Cohen, H.; Cohen, S.; Kjaer, K.; Howes, P. B.; Als-Nielsen, J.; Lehn, J.-M.; Leiserowitz, L.; Lahav, M. *Chem.—Eur. J.* **2000**, *6*, 725–734.
(18) Kuzmenko, I.; Rapaport, H.; Kjaer, K.; Als-Nielsen, J.; Weissbuch, I.; Lahav, M.; Leiserowitz, L. *Chem. Rev.* **2001**, *101*, 1659–1696.
(19) For the formation of other types of highly ordered materials, see: (a) Shirman, T.; Freeman, D.; Diskin Posner, Y.; Feldman, I.; Facchetti, A.; van der Boom, M. E. *J. Am. Chem. Soc.* **2008**, *130*, 8162–8163. (b) Kanaizuka, K.; Haruki, R.; Sakata, O.; Yoshimoto, M.; Akita, Y.; Kitagawa, H. *J. Am. Chem. Soc.* **2008**, *130*, 15778–15779.
(20) Gong, J.-R.; Wan, L.-J.; Yuan, Q.-H.; Bai, C.-L.; Jude, H.; Stang, P. J. *Proc. Natl. Acad. Sci. U. S. A.* **2005**, *102*, 971–974.
(21) Zheng, Y.-R.; Stang, P. J. *J. Am. Chem. Soc.* **2009**, *131*, 3487–3489.


Published on Web 09/02/2009

**Scheme 1. Two-Step Strategy for the Multilayer Formation with Complex 2 and Chromophores 3 or 4[a]**

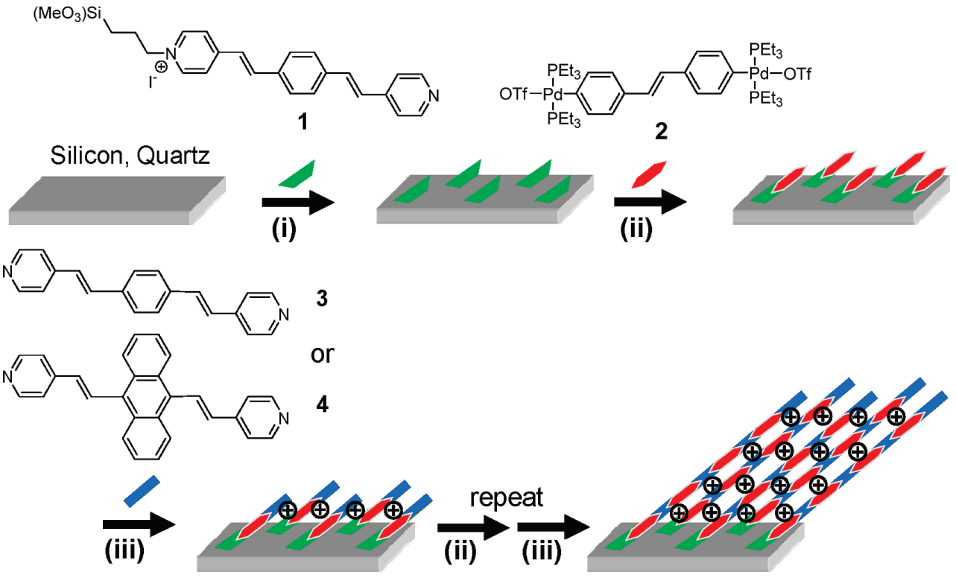


[a] The deposition is carried out under an inert atmosphere, but the resultant assembly is stable under ambient conditions based on UV-vis spectroscopy and ellipsometry. Charges as shown are not stoichiometric; charges in initial steps and counteranions are omitted for clarity.

that can be reversibly locked to act as a container molecule.[22,23] The variety of macromolecules and supramolecular structures that can be assembled from metal−organic building blocks seems boundless.[14,24,25] However, relatively few examples exist of organometallic or metal−organic supramolecular assemblies directly anchored from solution onto surfaces in a rational manner.[26] Various molecule-based solid-state assemblies have been formed via layer-by-layer deposition from solution.[27−37] Ordered multilayer assemblies based on the coordination of Zn, Hf, and Cu, among others, have been studied by various groups.[27,32,38−45] Remarkably, Fischer and Wöll demonstrated the stepwise growth of metal−organic frameworks (MOFs).[34,35] We recently reported on hybrid materials with molecular-layer precision and interesting properties, including self-propagating growth, electrochromic effects, and exciplex-type behavior.[28−31] In particular, metal−organic multilayers with a high degree of ordering in three dimensions were imparted by the highly specific coordination chemistry and in-plane $\pi-\pi$ interactions.[29] The use of well-defined organometallic complexes may be hampered by their reactivity under ambient conditions. However, the use of such complexes might offer useful synthons that have a precise coordination chemistry allowing the predesign of the solid-state order and charge distribution. Solid-state assemblies having localized charges are known to have significant optical and electronic properties.[31,46−49] It is interesting to compare the frontier orbitals of these materials with those of their neutral cogeners. This might allow rational control of

(22) Mal, P.; Schultz, D.; Beyeh, K.; Rissanen, K.; Nitschke, J. R. *Angew. Chem., Int. Ed.* **2008**, *47*, 8297–8301.
(23) Neyman, A.; Meshi, L.; Zeiri, L.; Weinstock, I. A. *J. Am. Chem. Soc.* **2008**, *130*, 16480–16481.
(24) Maspoch, D.; Ruiz-Molina, D.; Veciana, J. *Chem. Soc. Rev.* **2007**, *36*, 770–818.
(25) Saalfrank, R. W.; Maid, H.; Scheurer, A. *Angew. Chem., Int. Ed.* **2008**, *47*, 8794–8824.
(26) Li, S.-S.; Northrop, B. H.; Yuan, Q.-H.; Wan, L.-J.; Stang, P. J. *Acc. Chem. Res.* **2009**, *42*, 249–259.
(27) Lee, H.; Kepley, L. J.; Hong, H. G.; Akhter, S.; Mallouk, T. E. *J. Phys. Chem.* **1988**, *92*, 2597–2601.
(28) Altman, M.; Shukla, A. D.; Zubkov, T.; Evmenenko, G.; Dutta, P.; van der Boom, M. E. *J. Am. Chem. Soc.* **2006**, *128*, 7374–7382.
(29) Altman, M.; Zenkina, O.; Evmenenko, G.; Dutta, P.; van der Boom, M. E. *J. Am. Chem. Soc.* **2008**, *130*, 5040–5041.
(30) Motiei, L.; Lahav, M.; Freeman, D.; van der Boom, M. E. *J. Am. Chem. Soc.* **2009**, *131*, 3468–3469.
(31) Motiei, L.; Altman, M.; Gupta, T.; Lupo, F.; Gulino, A.; Evmenenko, G.; Dutta, P.; van der Boom, M. E. *J. Am. Chem. Soc.* **2008**, *130*, 8913–8915.
(32) Wanunu, M.; Popovitz-Biro, R.; Cohen, H.; Vaskevich, A.; Rubinstein, I. *J. Am. Chem. Soc.* **2005**, *127*, 9207–9215.
(33) van der Boom, M. E.; Evmenenko, G.; Yu, C.; Dutta, P.; Marks, T. J. *Langmuir* **2003**, *19*, 10531–10537.
(34) (a) Shekhah, O; Wang, H.; Zacher, D.; Fischer, R. A.; Wöll, C. *Angew. Chem., Int. Ed.* **2009**, *48*, 5038–5041. (b) Shekhah, O.; Wang, H.; Kowarik, S.; Schreiber, F.; Paulus, M.; Tolan, M.; Sternemann, C.; Evers, F.; Zacher, D.; Fischer, R. A.; Wöll, C. *J. Am. Chem. Soc.* **2007**, *129*, 15118–15119.
(35) Zacher, D.; Shekhah, O.; Wöll, C.; Fischer, R. A. *Chem. Soc. Rev.* **2009**, *38*, 1418–1429.
(36) Kuhn, H.; Ulman, A. *Thin Films* **1995**, *20*, 1–7.
(37) Netzer, L.; Sagiv, J. *J. Am. Chem. Soc.* **1983**, *105*, 674–676.
(38) Kanaizuka, K.; Haruki, R.; Sakata, O.; Yoshimoto, M.; Akita, Y.; Kitagawa, H. *J. Am. Chem. Soc.* **2008**, *130*, 15778–15779.
(39) Katz, H. E.; Scheller, G.; Putvinski, T. M.; Schilling, M. L.; Wilson, W. L.; Chidsey, C. E. D. *Science* **1991**, *254*, 1485–1487.
(40) Maoz, R.; Sagiv, J. *Adv. Mater.* **1998**, *10*, 580–584.
(41) van der Boom, M. E.; Evmenenko, G.; Dutta, P.; Marks, T. J. *Adv. Funct. Mater.* **2001**, *11*, 393–397.
(42) Hatzor, A.; Moav, T.; Cohen, H.; Matlis, S.; Libman, J.; Vaskevich, A.; Shanzer, A.; Rubinstein, I. *J. Am. Chem. Soc.* **1998**, *120*, 13469–13477.
(43) Moav, T.; Hatzor, A.; Cohen, H.; Libman, J.; Rubinstein, I.; Shanzer, A. *Chem.—Eur. J.* **1998**, *4*, 502–507.
(44) Cao, G.; Hong, H. G.; Mallouk, T. E. *Acc. Chem. Res.* **1992**, *25*, 420–427.
(45) Hatzor, A.; Weiss, P. S. *Science* **2001**, *291*, 1019–1020.
(46) Evmenenko, G.; van der Boom, M. E.; Kmetko, J.; Dugan, S. W.; Marks, T. J.; Dutta, P. *J. Chem. Phys.* **2001**, *115*, 6722–6727.
(47) Marks, T. J. *Angew. Chem., Int. Ed.* **1990**, *29*, 857–879.
(48) Usta, H.; Facchetti, A.; Marks, T. J. *J. Am. Chem. Soc.* **2008**, *130*, 8580–8581.
(49) Polyelectrolyte-based films consist of charged oligomers whose resulting matrix is fundamentally different in conception and order. See for examples: Decher, G.; Schlenoff, J. B. *Multilayer Thin Films: Sequential Assembly of Nanocomposite Materials*; Wiley-VCH: Weinheim, Germany, 2003.

**Scheme 2. Molecular Structure and Formation of Complex 2**[a]

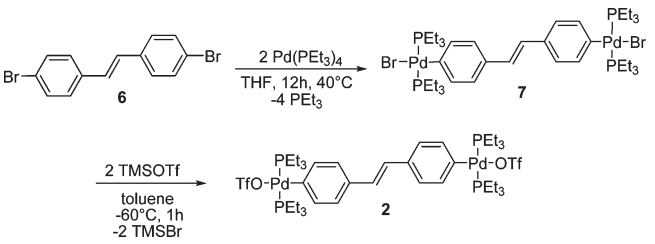


[a] The bimetallic precursor **7** was formed by aryl-Br activation with palladium (TMS = $Me_3Si$, OTf = $CF_3SO_3$).

the HOMO and LUMO levels of the system. Finally, the presence of such a high density of charges in a thin film, may result in effectively tunable surface states.

Here, we report on molecular-precise assemblies of surface-bound cationic palladium-based oligomers whose positive charges are isolated on the metal centers. These solution-based layer-by-layer formed "positive constructs" are built up from a well-defined organometallic complex and rigid-rod organic chromophores. The presence of the positive charge and/or steric hindrance of phosphine ligands apparently preclude $\pi-\pi$ interactions between the oligomers. Electronic communication does not occur along the molecular chains. The positively charged complexes remain isolated by the neutral organic chromophores in the well-defined assembly while continuing to transmit the structural information of the underlying layers.

## Results and Discussion

The assembly strategy consists of wet-chemical deposition (Scheme 1). Silicon and quartz substrates were functionalized with a **1**-based template layer, followed by alternate coordination of complex **2** and chromophore **3** or **4**. The template layer and chromophores **1**, **3**, and **4** have recently been reported by us and others.[28,29,50−52] The formation of complex **2** and a cationic model complex (**5**), mimicking the structure and properties of the solid-state oligomers, is described below.

**Formation of Complex 2.** The reaction of 1-bromo-4-[2-(4-bromophenyl)vinyl]-benzene (**6**) and 2 equiv of $Pd(PEt_3)_4$ in dry THF at 40 °C for 12 h results in the quantitative formation of the bimetallic complex **7** as determined by $^{31}P\{^1H\}$ NMR spectroscopy (Scheme 2). Complex **7** was isolated as a light yellow solid in 93% yield and fully characterized by $^1H$, $^{13}C\{^1H\}$, and $^{31}P\{^1H\}$ NMR spectroscopy, elemental analysis, and single-crystal X-ray crystallography (Figure 1). The $^{13}C\{^1H\}$ NMR spectrum shows a characteristic triplet resonance at $\delta$ = 155.82 ppm with $^2J_{PC}$ = 10.7 Hz, indicating a $\sigma$-bound aromatic carbon moiety coupled by two

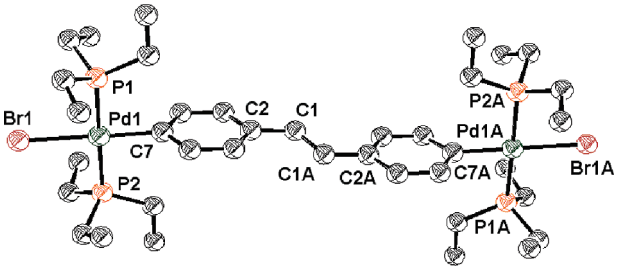


**Figure 1.** ORTEP diagram of complex **7** with thermal ellipsoids set at 50% probability. There is 1/2 molecule per asymmetric unit. Hydrogen atoms are omitted for clarity. Selected bond lengths [Å] and angles [deg]: Pd(1)−Br(1) 2.5178(3), Pd(1)−P(1) 2.2999(7), Pd(1)−P(2) 2.3156(7), Pd(1)−C(7) 2.010(3), C(2)−C(1) 1.478(4), C(1)−C(1A) 1.322(6), C(7)−Pd(1)−Br(1) 179.32(9), P(2)−Pd(1)−P(1) 178.99(3), C(7)−Pd(1)−P(1) 89.60(7). The arene carbon−carbon bond lengths are within the expected range of 1.379−1.403 Å. Atomic color scheme: (Br) red, (P) orange, (Pd) green, (C) black.

magnetically equivalent phosphorus atoms.[53,54] The $^{31}P\{^1H\}$ NMR spectrum exhibits one sharp singlet at $\delta$ 12.62 ppm for all $^{31}P$ nuclei, indicating that these atoms are magnetically equivalent. These spectroscopic features are consistent with complexes incorporating other transition metals or stilbene-like ligands.[50,53,55,56]

Yellow crystals of complex **7** were obtained upon slow evaporation of a THF/pentane (1:5 v/v) solution under a nitrogen atmosphere at room temperature. Single crystal X-ray analysis clearly shows the bimetallic nature (Figure 1), with a square planar geometry around the Pd(II) centers with corresponding angles of C(7)−Pd(1)−P(1) = 89.60°, C(7)−Pd(1)−Br(1) = 179.32°, and P(2)−Pd(1)−P(1) = 178.99°.

The reaction of complex **7** with 2 equiv TMSOTf in dry toluene at −60 °C for 40 min results in the quantitative formation of complex **2** as determined by $^{31}P\{^1H\}$ NMR spectroscopy (Scheme 2). TMSOTf was introduced by Milstein in 1994 as an efficient reagent to abstract halides from transition-metal complexes.[57] The resulting TMSBr is highly volatile and can be removed under vacuum. Stang employed this strategy to form platinum complexes used to assemble cationic macrocycles in solution.[58] Complex **2** was isolated in 83% yield as a dark orange solid and characterized by $^1H$, $^{19}F\{^1H\}$, and $^{31}P\{^1H\}$ NMR spectroscopy and by elemental analysis. The $^{31}P\{^1H\}$ NMR spectrum exhibits one singlet resonance at 13.76 ppm, whereas the $^{19}F\{^1H\}$ NMR spectrum shows a characteristic peak for both triflate anions at $\delta$ −77.44 ppm. Complex **2** is air sensitive in solution but stable as a powder at −40 °C under $N_2$ for at least 2 months.

**Formation of Model Complex 5.** The reaction of complex **2** with 2 equiv of 4-[2-[4-(2-phenylethenyl)phenyl]-

(50) Zenkina, O. V.; Konstantinovski, L.; Freeman, D.; Shimon, L. J. W.; van der Boom, M. E. *Inorg. Chem.* **2008**, *47*, 3815–3822.
(51) Detert, H.; Stalmach, U.; Sugiono, E. *Synth. Met.* **2004**, *147*, 227–231.
(52) Sokolov, T. N.; Friscic, T.; MacGillivray, L. R. *J. Struct. Chem.* **2005**, *46*, S171.
(53) Manna, J.; Kuehl, C. J.; Whiteford, J. A.; Stang, P. J. *Organometallics* **1997**, *16*, 1897–1905.
(54) Granell, J.; Muller, G.; Rocamora, M.; Vilarrasa, J. *Magn. Reson. Chem.* **1986**, *24*, 243–246.
(55) Beletskaya, I. P.; Chuchurjukin, A. V.; Dijkstra, H. P.; van Klink, G. P. M.; van Koten, G. *Tetrahedron Lett.* **2000**, *41*, 1075–1079.
(56) Cámpora, J.; Gutiérrez, E.; Poveda, M. L.; Ruíz, C.; Carmona, E. *J. Chem. Soc. Dalton* **1992**, 1769–1774.
(57) Aizenberg, M.; Milstein, D. *J. Chem. Soc. Chem. Commun.* **1994**, 411–412.
(58) Manna, J.; Kuehl, C. J.; Whiteford, J. A.; Stang, P. J.; Muddiman, D. C.; Hofstadler, S. A.; Smith, R. D. *J. Am. Chem. Soc.* **1997**, *119*, 11611–11619.

**Scheme 3. Formation of Model Complex 5**[a]

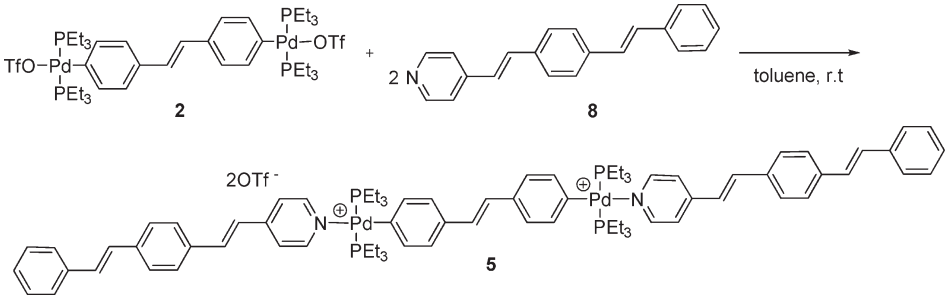


[a] This complex was used to demonstrate the feasibility of the coordination between similar chromophores (i.e., **3** and **4**) and complex **2** and afforded characterization in solution. The stability of complex **5** under ambient conditions reinforces the stability of the surface bound assemblies.

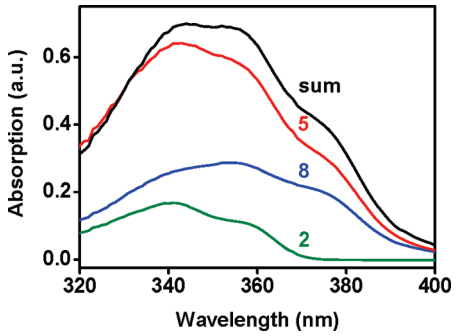


**Figure 2.** Absorption vs wavelength for complex **2** (green), chromophore **8** (blue), and model complex **5** (red) in toluene. For comparison, the arithmetical sum of the spectrum of complex **2** and twice the spectrum of chromophore **8** is also presented (black line). Significantly, it is almost identical to the spectrum of the model complex (**5**) indicating only minor changes in the electronic distribution upon coordination.

ethenyl]-pyridine (**8**) in toluene at 25 °C for ~15 min results in the quantitative formation of the cationic complex **5** (Scheme 3). All volatiles were removed in vacuo after 2 h. The compound was obtained in 86% yield by washing the residue with pentane. In contrast to precursor **2**, complex **5** was found to be stable as a powder under air for at least 2 months at room temperature according to $^{1}H$ and $^{31}P\{^{1}H\}$ NMR spectroscopy. Likewise, the surface-bound chromophore-terminated assemblies are stable under air as judged by optical spectroscopy (vide infra). The NMR data confirms that compound **8** is coordinated to the palladium centers of complex **2** via the pyridyl moieties. Metal coordination to the C=C bonds is not observed. $^{15}N$ NMR spectroscopy reveals that the signal of the nitrogen atoms of complex **5** is shifted relative to the signal of the free ligand (**8**) by only −9.9 ppm to $\delta$ 297.3 ppm. This indicates that the positive charge in this complex does not reside on the nitrogen atoms but likely remains localized on the metal.[59]

Interestingly, the UV−vis spectrum of complex **5** appears as the sum of the spectra of compound **8** (2×) and complex **2** with no evidence of electron delocalization due to changes in the conjugation length (Figure 2). The similarity between the absorption, $I$, of the macromolecular structure (**5**) and the sum of the absorption of the components (i.e., $I_2 + 2I_8$), indicates electron localization. By extension, we conjecture that the positive charges are localized on the metal atoms.

**Stepwise Formation of Organometallic-Based Positive Constructs.** The multilayer structure shown in Scheme 1 was obtained by iterative two-step deposition using **1**-based template layers covalently bound to quartz and silicon substrates. These substrates were functionalized with compound **1** using an adaptation of our previously reported method and identified by UV−vis spectroscopy, spectroscopic ellipsometry, and atomic force microscopy (AFM) imaging.[28,29] The **1**-functionalized substrates were immersed in a 1 mM solution of complex **2** in dry THF for 30 min at room temperature, rinsed with dry THF and allowed to dry. The entire procedure was performed in an $N_2$-filled glovebox. Subsequently, the samples were immersed for another 40 min in a 1 mM solution of compound **3** or **4** in THF at room temperature and rinsed. These two steps were repeated six times to form the assemblies. Although complex **2** is air-sensitive, the surface-bound oligomers and model complex **5** are stable when stored under ambient conditions as determined by UV−vis spectroscopy. The chromophores (**3** and **4**) were selected to evaluate the effect of possible $\pi-\pi$ interactions and the electronic contribution of the relatively large anthracene unit (**4**), as opposed to a single central phenyl ring (**3**). We previously showed that chromophore **4** coordinated to $PdCl_2$ forms a 3D-ordered multilayer through a combination of metal−ligand coordination and $\pi-\pi$ interactions,[29] whereas chromophore **3** forms discrete surface-bound molecular wires with $PdCl_2$ using identical deposition procedures.[28]

For both multilayers, the UV−vis absorption and the ellipsometrically determined thickness increase linearly with each addition deposition cycle (Figure 3). For the **3**-based system, the total ellipsometrically derived thickness of 55.6 Å is consistent with the thickness of 53.5 Å determined by synchrotron X-ray reflectivity (XRR) (Figures 3a and 4a). This implies a thickness along the normal of 8 Å for each bilayer of compounds **2** and **3**. Figure 3b shows the linear increase in ellipsometry-determined thickness with each additional bilayer ($R^2$ = 0.993) for the **4**-based multilayer. This provides strong evidence of the ordered and systematic assembly of this system as well. The ellipsometrically and XRR determined thicknesses of 41.2 Å (Figure 3b) and 38.5 Å

(59) Pazderski, L.; Szlyk, E.; Sitkowski, J.; Kamienski, B.; Kozerski, L.; Tousek, J.; Marek, R. *Magn. Reson. Chem.* **2006**, *44*, 163–170.

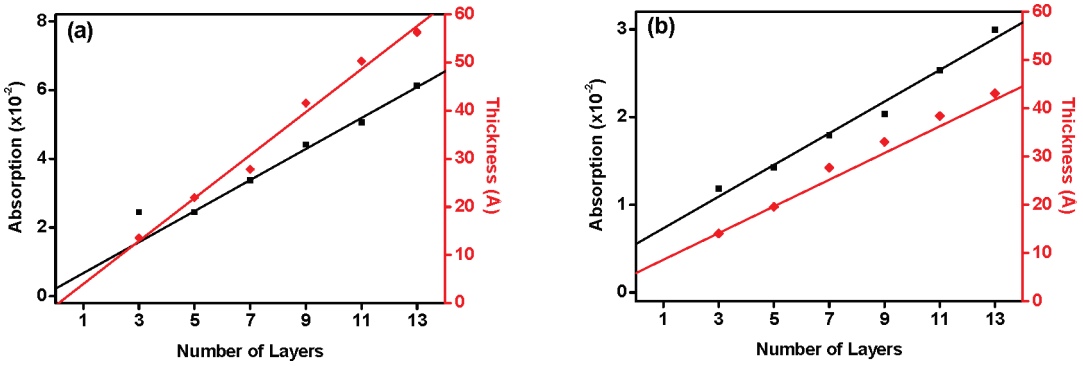


**Figure 3.** Linear growth as indicated by UV−vis spectroscopy and spectroscopic ellipsometry for chromophore-terminated films. (a) Optical absorption at $\lambda = 350$ nm (■, $R^2 = 0.996$, left axis) and ellipsometrically determined thickness (◆, red, $R^2 = 0.988$, right axis) for a **3**-based multilayer on quartz and silicon, respectively. (b) Optical absorption at $\lambda = 350$ nm (■, $R^2 = 0.983$, left axis) and ellipsometrically determined thickness (◆, red, $R^2 = 0.994$, right axis) for **4**-based multilayer on quartz and silicon, respectively. For both multilayers, the **1**-based template layer was excluded from the linear regression. The UV−vis spectra of both systems were also integrated and the total area under the curve vs number of deposition cycles shows the same linear trend.

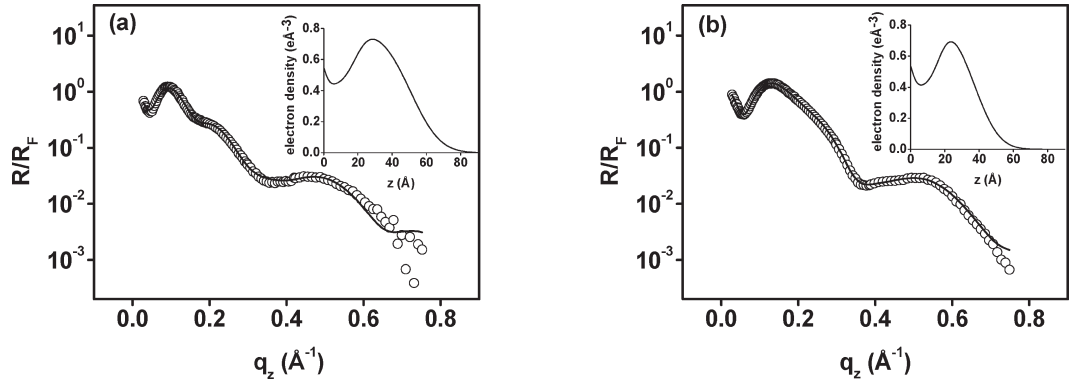


**Figure 4.** XRR spectra for six deposition cycles of (a) the **3**-based multilayer and (b) the **4**-based multilayer. The line is a fit based on a previously described model.[46] (insets) Electron density plots of the XRR data for parts a and b.

(Figure 4b), respectively, for the **4**-based system are actually lower by about a third relative to the **3**-based system. This is despite the additional volume that the additional rings in the anthracene core would be expected to occupy. According to the increase in thickness of both assemblies, the films are growing at an average angle of ~10°, relative to the surface, using density functional theory (DFT) estimates of the lengths of 16.2 Å for chromophores **3** and **4**, and 13.5 Å for complex **2**. The direction of growth may be attributed to a combination of the orientation of the template layer and charge repulsion.[28]

The XRR determined roughness of the **3**-based assembly is 8 Å, similar to the 5 Å observed for the **4**-based assembly. The electron density is around 0.5 eÅ$^{-3}$ for both films (Figure 4, insets). This is similar to the values reported for other organized coordination-based multilayer films.[28,29] Figure 4a and b shows an initial distinct Kiessig fringe, but subsequent fringes are suppressed. Their effective thickness varies with $\sigma$ = 10 Å. This corresponds to half-width of Gaussian at level $\sigma = 0.61$, which results in a full width for the Gaussians of ~40 Å. This is supported by the grainy structure of the films observed by AFM (vide infra, Figure 5).

A semicontact AFM image of the **3**-based assembly is shown in Figure 5a. The roughness ($R_{rms}$ = 0.6 nm), similar to that observed by XRR (vide supra), is low relative to both the template layer and to other molecular-based multilayer assemblies.[28,32] Nevertheless, the image shows some graininess, with gaps with apparent depths of ~4 nm. These reflect the morphology of the underlying template layer rather than defects in the multilayer assembly.[28] The template layer was consistent for both assemblies. Since the width of the holes is of the order of magnitude of the ~10 nm radius of the AFM tip,[28,60,61] the nominal depth is less than the thickness of the entire assembly. This might open the possibilities to generate structurally precise assemblies on **1**-based patterned templates.[28,62−67] The semicontact AFM image of the **4**-based assembly is shown in Figure 5b. The surface appears grainy, without any salient features and with a moderate roughness of 1.5 nm, which is higher than the 0.5 nm determined by XRR. This apparently reflects

(60) Zubkov, T.; Lucassen, A. C. B.; Freeman, D.; Feldman, Y.; Cohen, S. R.; Evmenenko, G.; Dutta, P.; van der Boom, M. E. *J. Phys. Chem. B.* **2005**, *109*, 14144–14153.
(61) Takahashi, T.; Takei, K.; Ho, J. C.; Chueh, Y.-L.; Fan, Z.; Javey, A. *J. Am. Chem. Soc.* **2009**, *131*, 2102–2103.
(62) Collins, R. J.; Shin, H.; DeGuire, M. R.; Heuer, A. H.; Sukenik, C. N. *Appl. Phys. Lett.* **1996**, *69*, 860–862.
(63) Buxboim, A.; Bar-Dagan, M.; Frydman, V.; Zbaida, D.; Morpurgo, M.; Bar-Ziv, R. *Small* **2007**, *3*, 500–510.
(64) Crespo-Biel, O.; Dordi, B.; Maury, P.; Peter, M.; Reinhoudt, D. N.; Huskens, J. *Chem. Mater.* **2006**, *18*, 2545–2551.
(65) Ling, X. Y.; Phang, I. Y.; Reinhoudt, D. N.; Vancso, G. J.; Huskens, J. *Int. J. Mol. Sci.* **2008**, *9*, 486–497.
(66) Park, J.; Hammond, P. T. *Adv. Mater.* **2004**, *16*, 520–525.
(67) Park, J.; Kim, I.; Shin, H.; Lee, M. J.; Kim, Y. S.; Bang, J.; Caruso, F.; Cho, J. *Adv. Mater.* **2008**, *20*, 1843–1848.

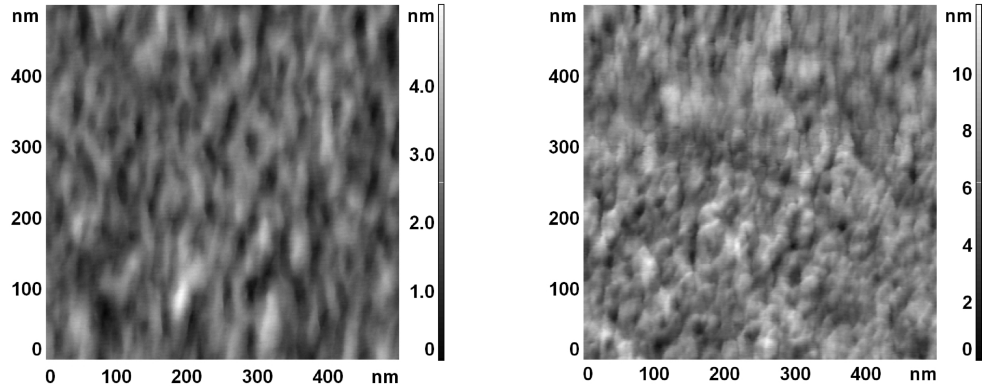


**Figure 5.** Semicontact AFM images of a 500 nm × 500 nm scan area on silicon of a (a) **3**-based multilayer ($R_{rms}$ = 0.64 nm; peak-to-peak: 5.2 nm) and (b) **4**-based multilayer ($R_{rms}$ = 1.5 nm; peak-to-peak: 12.4 nm).

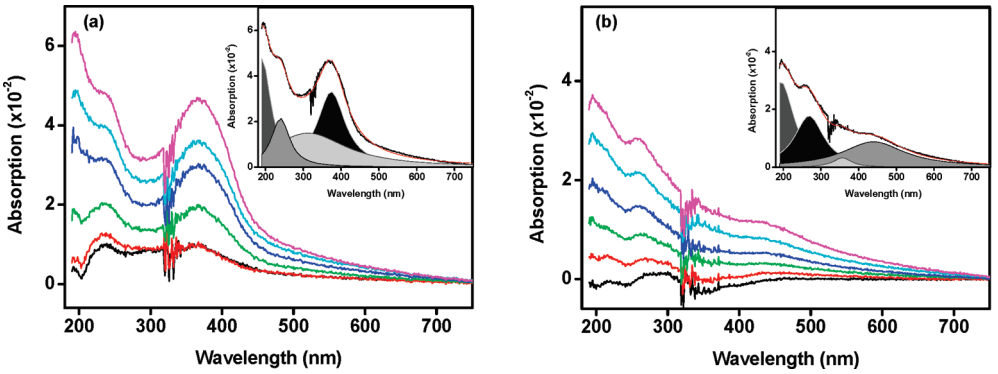


**Figure 6.** Absorption vs wavelength for 3 (black), 5 (red), 7 (green), 9 (dark blue), 11 (light blue), and 13 (pink) layers on quartz of the (a) **3**-based multilayer and (b) **4**-based multilayer. The baseline drift for both systems was corrected in the visible range and the absorption of the **1**-based template layer was subtracted from subsequent layers. (insets) Laurenzian deconvolution for six deposition cycles illustrating the proposed bands of the assembly components.

the microscructure rather than the local roughness. The difference in the roughness values can be attributed to the inherent difference between the two methods.

Figure 6a shows the UV−vis spectroscopic traces of the multilayer formed from complex **2** and chromophore **3** after subtraction of the absorption of the template layer. The principle absorption peak at 350 nm corresponds to chromophore **3**, and it increases linearly with each additional deposition cycle (Figure 3a). The peaks are relatively broad, as would be expected for surface-bound molecules or assemblies.[28,68] In contrast with the previously reported coordination-based assembly of compound **3** and $PdCl_2$, Figure 6a shows that the position of the adsorption maximum of this peak remains constant.[28] This indicates that for the current system there is no increase in the conjugation length with the increase in physical length of the surface bound oligomers. This is in agreement with the optical properties of model complex **5** (Figure 2). A ligand-to-metal charge-transfer (LMCT) band appears as a shoulder in the range 257−260 nm, which also increases linearly with each additional ligand−complex deposition cycle. A multipeak fit of the data suggests bands located at 191, 240, 313, and 374 nm (Figure 6a inset) with $R^2$ = 0.996. These values for the bands associated with the Pd-ligand LMCT (241 nm) and with chromophore **3** (371 nm) are consistent with our previous work.[28] The retention of these bands upon assembly is consistent with a system that does not undergo significant electron delocalization.

The UV−vis absorption for the **4**-based multilayer assembly is presented in Figure 6b. There is also an increase in the absorption with each additional layer as confirmed by the linear regression presented in Figure 3b. In contrast to the **3**-based system, no sharp bands are evident due to overlap and convolution. As a result, the spectra in Figure 6b resemble wavy diagonal lines where the increase with each cycle is linear at almost every wavelength in the range of 200−700 nm. Furthermore, the absorption intensity of the system is less than for the **3**-based assembly; the $\varepsilon$ of chromophore **4** in dioxane ($1.4 \times 10^4$ cm$^{-1}$ M$^{-1}$, $\lambda$ = 412 nm) is lower than that of chromophore **3** ($3.6 \times 10^4$ cm$^{-1}$ M$^{-1}$, $\lambda$ = 352 nm). This can be attributed to the lack of conjugation in the nonplanar chromophore **4** which possesses steric hindrance between the hydrogens of the anthracene core and those of the ethylene bridge.[29] The inset of Figure 6b shows the deconvolution of the UV−vis absorption before normalization.[69] This treatment reveals

(68) Gupta, T.; van der Boom, M. E. *Angew. Chem., Int. Ed.* **2008**, *47*, 5322–5326.

(69) Hosomizu, K.; Oodoi, M.; Umeyama, T.; Matano, Y.; Yoshida, K.; Isoda, S.; Isosomppi, M.; Tkachenko, N. V.; Lemmetyinen, H.; Imahori, H. *J. Phys. Chem. B* **2008**, *112*, 16517–16524.

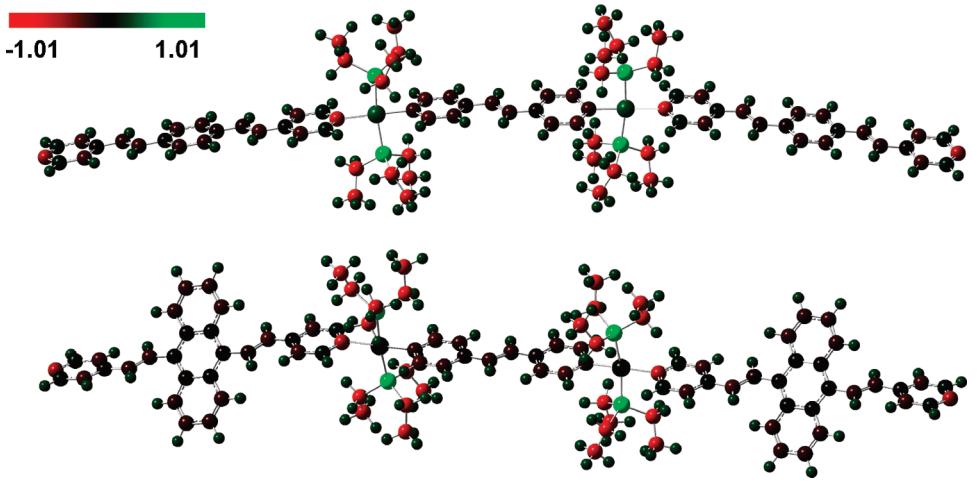


**Figure 7.** Natural population analysis (NPA) charges of the **3**−**2**−**3** (top) and **4**−**2**−**4** (bottom) sequences showing the positive charge that is mostly isolated on the palladium and phosphine atoms of the complex **2** unit.

that the trace is composed of individual peaks at or around 194, 267, 356, and 439 nm ($R^2 = 0.994$). Although the fit is numerically strong, the peak positions represent an approximation because of the broadness of the bands. Therefore, intermolecular interaction in this system cannot be excluded. We have shown that compound **4** and $PdCl_2$ form 3D-ordered assemblies because of strong chromophore−chromophore interactions with large changes in the optical data.[29]

DFT modeling using the M06 functional supports the notion that there is no electron delocalization along the oligomers. Calculations on **3**−**2**−**3** (c.f. complex **5**) and **4**−**2**−**4** show that the positive charge resides mostly on the palladium−phosphine moieties. For example, for the **3**−**2**−**3** sequence (Figure 7), the charges on palladium and phosphine are +0.28 and +0.98, respectively. By contrast, on compound **3,** negative charges of −0.61 and −0.51 are recorded for the bound and unbound pyridyl nitrogens, respectively. No significant positive charge resides on the carbon or hydrogen atoms in the system either (−0.27 to +0.9 and 0.22, respectively). Similar values were obtained for the **4**−**2**−**4** structure. The cationic charges present in complex **2** remain localized and effectively trapped, even after coordination of compound **3** or **4** (despite the apparent conjugation in the individual components **2** and **3**). This is in contrast to our previously reported assemblies where the coordination of chromophore **3** to $PdCl_2$ did not detract from the conjugation in the system.[28,29]

The HOMO−LUMO gap calculated by DFT for the **3**−**2**−**3** oligomer is 3.02 eV. This compares favorably with the experimental optical band gap ($E_{opt}$) for the assembly of 3.42 eV. Similarly, the DFT HOMO−LUMO gap for the **4**−**2**−**4** oligomer is 2.60 eV, while the $E_{opt}$ is 2.82 eV. This is less than for the **3**-based system and lower than reported for other metal−organic assemblies.[70]

## Summary and Conclusions

Multilayer assemblies consisting of organometallic palladium complexes have been formed with molecular-level precision. Coordination of a bimetallic complex to pyridine-terminated chromophores by iterative deposition results in multivalent cationic surface-bound oligomers. While the sensitivity of the bimetallic precursor requires that the structures be prepared under the strict exclusion of air, the resulting positive constructs are stable under ambient conditions. The linear growth of the assemblies is consistent with the formation of a structured film. Deconvolution of the UV−vis spectra reveals that the absorption bands of the individual film components can be discerned in the overall assembly with no evident electron delocalization. This is supported by DFT calculations and the optical properties in solution of a model complex. The DFT calculations also show that the HOMO and LUMO levels of these oligomers are lower than for neutral analogs. These assemblies demonstrate the breadth and generality of our layer-by-layer assembly strategy to form materials with new optical and structural properties.[28,29,31,49] While a high degree of structural communication is preserved, our observations imply that there is no axial electronic communication across the assembly. As a result, the palladium complexes are electronically isolated. These cationic oligomers could provide insight into the behavior of more complex surface-bound charged systems or capacitorlike molecular matrices.[71−75]

(70) Gascon, J.; Hernández-Alonso, M. D.; Almeida, A. R.; van Klink, G. P. M.; Kapteijn, F.; Mul, G. *ChemSusChem* **2008**, *1*, 981–983.
(71) Ray, S. G.; Cohen, H.; Naaman, R.; Rabin, Y. *J. Am. Chem. Soc.* **2005**, *127*, 17138–17139.
(72) Alam, M. S.; Strömsdörfer, S.; Dremov, V.; Müller, P.; Kortus, J.; Ruben, M.; Lehn, J.-M. *Angew. Chem., Int. Ed.* **2005**, *44*, 7896–7900.
(73) Snow, E. S.; Perkins, F. K.; Houser, E. J.; Badescu, S. C.; Reinecke, T. L. *Science* **2005**, *307*, 1942–1945.
(74) DiBenedetto, S. A.; Facchetti, A.; Ratner, M. A.; Marks, T. J. *Adv. Mater.* **2009**, *21*, 1407–1433.
(75) Hutchison, G. R.; Ratner, M. A.; Marks, T. *J. Phys. Chem. B.* **2005**, *109*, 3126–3128.

## Experimental Section

Compounds **1**, **3**, **4**, **6**, **8**, and $Pd(PEt_3)_4$ were prepared according to published procedures.[28,29,50,75−81] Reagents were purchased from Aldrich or Merck and used as received. Solvents were reagent grade (AR) from either Bio-Lab (Jerusalem, Israel), Merck (Darmstadt, Germany), or Baker Mallinckrodt (Phillipsburg, NJ). Tetrahydrofuran (THF) was distilled under $N_2$ over Na and degassed before introduction into an M. Braun glovebox. Single-crystal silicon ⟨100⟩ substrates, purchased from Wafernet (San Jose, CA), were cleaned by sonication in hexane followed by acetone and then ethanol and dried under an $N_2$ stream. Subsequently, they were cleaned for 20 min with UV and ozone in a UVOCS cleaning system (Montgomery, PA). Quartz slides (Chemglass, Vineland, NJ) were cleaned by immersion in a hot (70 °C) "piranha" solution (7:3 (v/v) $H_2SO_4$/30% $H_2O_2$) for 1 h. ***Caution!*** *Piranha solution is an extremely dangerous oxidizing agent and should be handled with care using appropriate personal protection*. The substrates were then rinsed with deionized water followed by the RCA cleaning protocol: 1:5:1 (v/v) $NH_3 \cdot H_2O$/$H_2O$/30% $H_2O_2$ at room temperature for 45 min.[33] The substrates were subsequently washed with deionized water and dried under an $N_2$ stream and then in an oven for 2 h at 130 °C. Template layer formation and preparation of metal complexes was carried out using dry solvents under an inert atmosphere using standard Schlenk/cannula techniques and an $N_2$-filled glovebox. UV−vis spectroscopy was carried out using a Cary 100 spectrophotometer. Atomic force microscopy (AFM) images were recorded using a Solver P47 (NT-MDT, Russia) operated in the semicontact mode. The cantilevers used were ultrasharp silicon (Olympus, Estonia) with a resonant frequency of ∼475 kHz and a tip radius of ∼10 nm. Roughness data ($R_{rms}$) were extracted from 500 nm × 500 nm images. Thickness was estimated using a J.A. Woollam (Lincoln, NB) model M-2000 V variable angle spectroscopic ellipsometer with VASE32 software. Measurements were performed on silicon at 2° intervals between 65 and 75° over a range of 399−1000 nm. A Cauchy model, with parameters $A$ = 1.55 and $B$ = 0.01, was used. The $^1H$, $^{13}C\{^1H\}$, $^{19}F\{^1H\}$, and $^{31}P\{^1H\}$ NMR spectra were recorded at 500.13, 125.77, 470.56, and 202.46 MHz, respectively, on a Bruker Avance 500 NMR spectrometer; $^{15}N-^1H$ NMR was recorded at 40.55 MHz on a Bruker Avance 400 NMR spectrophotometer. All chemical shifts ($\delta$) are reported in parts per million, and coupling constants ($J$), in hertz. The $^1H$ and $^{13}C$ NMR chemical shifts are relative to tetramethylsilane; $^{15}N$ NMR chemical shifts were referenced to liquid $NH_3$. The resonance of the residual protons of the solvent was used as the internal standard for $^1H$ NMR spectroscopy (7.15 ppm, benzene; 7.09 ppm, toluene; 5.32 ppm; methylene chloride), and the all-*d* solvent peaks were the standard for $^{13}C\{^1H\}$ NMR spectroscopy (128.0 ppm, benzene; 20.4 ppm, toluene; 53.8 ppm, methylene chloride). All measurements were carried out at 298 K. The 2D $^{15}N-^1H$ gsHMBC inverse proton detected heteronuclear shift correlation spectra were acquired and processed using standard Bruker software.[82]

**Formation of Complex 7.** A solution of $Pd(PEt_3)_4$ (66.9 mg, 0.116 mmol) in 4 mL of THF was added dropwise to the THF (4 mL) solution of 1-bromo-4-[2-(4-bromophenyl)vinyl]benzene (**6**) (19.5 mg, 0.0577 mmol). The solution was protected from light with aluminum foil and heated at 40 °C for 12 h resulting in the quantitative formation of complex **2** as determined by $^{31}P\{^1H\}$ NMR spectroscopy. All volatiles were removed under vacuum, and the remaining solid was washed with 5 mL of cold (−40 °C) pentane and dried in vacuo. Complex **7** was collected as a light yellow solid (55 mg, 93% yield). The yellow residue was redissolved in ∼2 mL of THF, which was followed by dropwise addition of ∼10 mL of pentane. Slow evaporation of the solvent at room temperature resulted after 7 days in the formation of yellow crystals suitable for X-ray diffraction. For **7**: $^1H$ NMR ($C_6D_6$): $\delta$ 7.35 (d, 2H, ArH, $^3J_{HH}$ = 7.4 Hz), 7.24 (d, 2H, ArH, $^3J_{HH}$ = 7.8 Hz), 7.13 (s, CH═CH, 2H), 1.53 (m, 24H, $PCH_2CH_3$), 0.91 (m, 36H, $PCH_2CH_3$). $^{13}C\{^1H\}$ NMR ($C_6D_6$): $\delta$ 155.82 (t, $C_q$, $^2J_{PC}$ = 10.7 Hz), 137.0 (s), 132.47 (s, $C_q$), 128.07, 125.62, 15.73 (vt, $PCH_2CH_3$, $^{1+3}J_{PC}$ = 13.1 Hz), 8.01 (s, $PCH_2CH_3$,). $^{31}P\{^1H\}$ NMR ($C_6D_6$): $\delta$ 12.62 (s, 4P). Elemental analysis (%) calcd for $C_{38}H_{70}Br_2N_3P_4Pd_2$: C, 44.59; H, 6.89. Found: C, 44.40; H, 7.34.

**X-ray Analysis of Complex 7.** Crystal data: $C_{38}H_{70}Br_2P_4Pd_2$, yellow, prisms, 0.1 × 0.1 × 0.4 $mm^{-3}$, monoclinic, $P2(1)/n$, $a$ = 9.4541(3) Å, $b$ = 13.3285(5) Å, $c$ = 15.0644(5) Å, $\beta$ = 90.212(1)°, $T$ = 100(2) K, $V$ = 2325.49(13) $Å^3$, $Z$ = 2, $F_w$ = 1023.44, $D_c$ = 1.462 Mg $m^{-3}$, $\mu$ = 2.652 $mm^{-1}$. Data collection and processing: Bruker Appex2 KappaCCD diffractometer, Mo Kα ($\lambda$ = 0.71073 Å), graphite monochromator, 26448 reflections collected, $-12 \le h \le 12$, $-17 \le k \le 23$, $-21 \le l \le 21$, 7157 independent reflections ($R_{int}$ = 0.0409). The data were processed with APEX2. Solution and refinement: The structure was solved by direct methods with SHELXS-97.[83] The full matrix least-squares refinement is based on $F^2$ with SHELXL-97. 214 parameters with 0 restraints, final $R_1$ = 0.0340 (based on $F^2$) for data with $I > 2\sigma(I)$ and $R_1$ = 0.0506 on 7141 reflections, goodness-of-fit on $F^2$ = 1.027, largest electron density peak = 1.592 e $Å^{-3}$.

**Formation of Complex 2.** A solution of complex **7** (51.0 mg, 0.0498 mmol) in 5 mL of toluene at −60 °C was added dropwise under stirring to a toluene (3 mL, −60 °C) solution of TMSOTf (22.1 mg, 0.0995 mmol). The reaction mixture was stirred at −60 °C for 40 min. All volatiles were then removed in vacuo. Washing the residue with cold pentane (−40 °C, ∼5 mL) afforded the analytically pure complex **2** as a dark orange solid in 83% yield. $^1H$ NMR ($C_6D_6$): $\delta$ 7.35 (d, 2H, ArH, $^3J_{HH}$ = 7.5 Hz), 7.23 (d, 2H, ArH, $^3J_{HH}$ = 7.8 Hz), 7.14 (m, CH═CH, 2H), 1.52 (m, 24H, $PCH_2CH_3$), 0.92 (m, 36H, $PCH_2CH_3$). $^{19}F\{^1H\}$ NMR ($C_6D_6$): $\delta$ −77.44 (s, OTf). Elemental analysis (%) calcd for $C_{40}H_{70}Pd_2P_4F_6O_6S_2$: C, 41.35; H, 6.07. Found: C, 41.30; H, 6.08.

**Formation of Model Complex 5.** A solution of complex **2** (20.0 mg, 0.172 mmol) in 2 mL of dry toluene was added dropwise to a solution of chromophore **8** (9.76 mg, 0.0344 mmol) in 2 mL of dry toluene and stirred at room temperature for 2 h. All volatiles were removed in vacuo after 2 h and the residue was washed with ∼3 mL of pentane. Compound **5** was obtained as a light yellow powder in 86% yield and is stable under air for at least 2 months. $^1H$ NMR ($CD_2Cl_2$): $\delta$ 8.59 (d, PyrH, $^3J_{HH}$ = 5.7 Hz), 7.62−7.59 (br, ArH), 7.50 (br, ArH), 7.42 (d, ArH, $^3J_{HH}$ = 7.1 Hz), 7.38 (d, ArH, $^3J_{HH}$ = 6.9 Hz), 7.34−7.30 (br, ArH), 7.26 (br, CH═CH), 7.23

(76) Das, A.; Maher, J. P.; McCleverty, J. A.; Navas Badiola, J. A.; Ward, M. D. *J. Chem. Soc., Dalton Trans.* **1993**, 681–686.
(77) Drefahl, G.; Plotner, G.; Buchner, G. *Chem. Ber.* **1961**, *94*, 1824–1833.
(78) Baker, B. R.; Gibson, R. E. *J. Med. Chem.* **1971**, *14*, 315–322.
(79) Barlow, S.; Risko, C.; Coropceanu, V.; Tucker, N. M.; Jones, S. C.; Levi, Z.; Khrustalev, V. N.; Antipin, M. Y.; Kinnibrugh, T. L.; Timofeeva, T.; Marder, S. R.; Bredas, J.-L. *Chem. Commun.* **2005**, 764–766.
(80) Sengupta, S.; Bhattacharyya, S.; Sadhukhan, S. K. *J. Chem. Soc., Perkin Trans. 1* **1998**, 275–278.
(81) Schunn, R. A. *Inorg. Chem.* **1976**, *15*, 208–212.
(82) von Philipsborn, W.; Müller, R. *Angew. Chem., Int. Ed.* **1986**, *25*, 383–413.
(83) Sheldrick, G. M. *SHELXL-97, Program for Crystal Structure Determination*; University of Göttingen: Göttingen, Germany, 1997.

(d, CH=CH, $^3J_{HH}$ = 17.7 Hz), 7.21 (d, CH=CH, $^3J_{HH}$ = 14.1 Hz), 7.16 (d, CH=CH, $^3J_{HH}$ = 17.1 Hz), 7.13 (d, CH=CH, $^3J_{HH}$ = 16.6 Hz), 6.98 (s), 1.63 (m, 24H, $PCH_2CH_3$), 1.11 (m, 36H, $PCH_2CH_3$). $^{13}C\{^1H\}$ NMR ($CD_2Cl_2$): $\delta$ 155.18 (t, $C_q$, $^2J_{PC}$ = 11.4 Hz), 149.86 (s), 137.0 (t, $^3J_{PC}$ = 4.1 Hz), 132.37 (s, $C_q$), 129.67 (s), 129.11 (s), 129.02 (s), 128.64 (s), 128.60 (s), 128.25 (s), 128.22 (s), 128.16 (s), 128.03 (s), 127.87, 127.30, 126.99 (s, $C_q$), 125.9.0 (s), 125.88 (s), 124.73 (s, $C_q$), 121.3 (s), 114.9 (s, $C_q$), 15.1 (vt, $PCH_2CH_3$, $^{1+3}J_{PC}$ = 13.1 Hz), 8.28 (s, $PCH_2CH_3$). $^{15}N$ NMR ($CD_2Cl_2$): $\delta$ 297.34. $^{19}F\{^1H\}$ NMR ($C_6D_6$): $\delta$ −79.09 (s, OTf). $^{31}P\{^1H\}$ NMR ($C_6D_6$): $\delta$ 13.16 (s, 4P).

**Template Layer Formation.** A modified version of a previously reported procedure was used to form the template layer.[28] Freshly cleaned quartz and silicon substrates (2.5 cm × 0.8 cm) were loaded into a Teflon sample holder that was loaded with a THF solution of compound **1** (0.35 mM) and heated at 77 °C for 8 h in a sealed pressure vessel with the exclusion of light. The functionalized substrates were then rinsed repeatedly with THF and sonicated in THF followed by acetone and ethanol for 6 min each. The substrates were dried under a stream of $N_2$. The assembly process was carried out in a single reaction vessel using standard cannula techniques.

**Multilayer Assembly with Complex 2 and Chromophore 3 or 4.** In an $N_2$-filled glovebox, cleaned quartz and silicon substrates functionalized with chromophore **1** were immersed in a 20 mL vial filled with a 1 mM solution of complex **2** in THF for 30 min. The samples were then rinsed twice in THF and allowed to dry. Subsequently, the samples were immersed for 40 min in a 1 mM solution of compound **3** or **4** in THF. The samples were then rinsed twice in THF and allowed to dry. The samples were then removed from the glovebox for analysis by UV−vis spectroscopy and ellipsometry. The chromophore terminated films are stable in air and growth was resumed unhindered following reintroduction into the glovebox. The procedure was repeated six times. The samples were stored in an $N_2$-filled glovebox before further analysis.

**Computational Details.** All calculations were carried out using Gaussian 03, revision E.01[84] to which the MNGFM patch was applied;[85] this patch from the University of Minnesota adds the M06 (vide infra) family of DFT exchange-correlation functionals to the commercial version. Two DFT exchange-correlation functionals were used. The first is the new M06 functional,[86] a meta-hybrid functional containing 27% HF exchange, which was shown to have superior performance in the study of transition metal reactions.[86,87] The second is the local version of the M06 family (M06-L).[88] This functional was shown to provide similar performance as M06 for transitional metals.[86,87]

With this functional, two basis set-RECP (relativistic effective core potential) combinations were used. The first, denoted SDD-(d), is the combination of the Huzinaga−Dunning double-ζ basis set[89] on lighter elements with the Stuttgart−Dresden basis set-RECP combination[90] on transition metals; an additional polarization function (i.e., the D95(d) basis set) was used on P atoms.

The second, denoted SDB-pc1, combines Jensen's pc-1 basis set[91−96] on the main group elements and the Stuttgart−Dresden basis set-RECP[90] on the transition metals with an added *f*-type polarization exponent taken as the geometric average of the two *f*-exponents given in the appendix of ref 97.

Density fitting basis sets (DFBS), as implemented in Gaussian03,[98] were employed in order to improve the computational efficiency of the calculation. Because the use of DFBSs precludes the use of a hybrid DFT exchange-correlation functional, the local version of the M06 family (M06-L) was employed.[88] This functional was shown to provide similar performance as M06 for transitional metals.[86,87] Truhlar recently recommended its use in such a scheme for optimizing large complexes followed by energy calculations with either M06 or M06-2X as appropriate (the former in this case because of the presence of a transition metal). The automatic DFBS generation algorithm built-in to Gaussian03 was employed. For interpretive purposes, natural population analysis (NPA) charges were derived from natural bond order (NBO) analyses calculated at the M06/SDB-pc1//M06-L/SDD(d)/DFBS level of theory.[99]

**Acknowledgment.** This research was supported by the Helen and Martin Kimmel Centers for Molecular Design and Nanoscale Science, the G. M. J. Schmidt Minerva Center, and the Weizmann−UK joint research program. X-ray reflectivity measurements were performed at Beamlines X6B and X18A of the National Synchrotron Light Source, which are supported by the U.S. Department of Energy. G.E. and P.D. were supported by the U.S. Department of Energy under Grant No. DE-FGO2-84ER45125. We thank Dr. G. Leitus and Dr. L. Konstantinovski from the Department of Chemical Research Support (WIS) for the X-ray structure determination of complex **7** and $^{15}N$ NMR experiments, respectively. Dr. D. Freeman from the Department of Organic Chemistry (WIS) prepared compound **8**.

**Supporting Information Available:** Full coordinates in .xyz format of calculated structures and crystallographic data for complex **7**. This material is available free of charge via the Internet at http://pubs.acs.org.

(84) Frisch, M. J.; Trucks, G. W.; Schlegel, H. B.; Scuseria, G. E.; Robb, M. A.; Cheeseman, J. R.; Montgomery, J. A., Jr.; Vreven, T.; Kudin, K. N.; Burant, J. C.; Millam, J. M.; Iyengar, S. S.; Tomasi, J.; Barone, V.; Mennucci, B.; Cossi, M.; Scalmani, G.; Rega, N.; Petersson, G. A.; Nakatsuji, H.; Hada, M.; Ehara, M.; Toyota, K.; Fukuda, R.; Hasegawa, J.; Ishida, M.; Nakajima, T.; Honda, Y.; Kitao, O.; Nakai, H.; Klene, M.; Li, X.; Knox, J. E.; Hratchian, H. P.; Cross, J. B.; Bakken, V.; Adamo, C.; Jaramillo, J.; Gomperts, R.; Stratmann, R. E.; Yazyev, O.; Austin, A. J.; Cammi, R.; Pomelli, C.; Ochterski, J. W.; Ayala, P. Y.; Morokuma, K.; Voth, G. A.; Salvador, P.; Dannenberg, J. J.; Zakrzewski, V. G.; Dapprich, S.; Daniels, A. D.; Strain, M. C.; Farkas, O.; Malick, D. K.; Rabuck, A. D.; Raghavachari, K.; Foresman, J. B.; Ortiz, J. V.; Cui, Q.; Baboul, A. G.; Clifford, S.; Cioslowski, J.; Stefanov, B. B.; Liu, G.; Liashenko, A.; Piskorz, P.; Komaromi, I.; Martin, R. L.; Fox, D. J.; Keith, T.; Al-Laham, M. A.; Peng, C. Y.; Nanayakkara, A.; Challacombe, M.; Gill, P. M. W.; Johnson, B.; Chen, W.; Wong, M. W.; Gonzalez, C.; Pople, J. A. Gaussian 03, revision E.01; Gaussian, Inc.: Wallingford, CT, **2004**.
(85) Zhao, Y.; Truhlar, D. G. with assistance from Iron, M. A.; Martin, J. M. L. Minnesota Gaussian Functional Module, version 3.1; University of Minnesota, Minneapolis, MN, **2008**.
(86) Zhao, Y.; Truhlar, D. G. *Theor. Chem. Acc.* **2008**, *120*, 215–241.
(87) Zhao, Y.; Truhlar, D. G. *Acc. Chem. Res.* **2008**, *41*, 157–167.
(88) Zhao, Y.; Truhlar, D. G. *J. Chem. Phys.* **2006**, *125*, 194101.
(89) Dunning, T. H., Jr.; Hay, P. J. *Modern Theoretical Chemistry*; Plenum: New York, 1976.
(90) Dolg, M. In *Modern Methods and Algorithms of Quantum Chemistry*; John von Neumann Institute for Computing: Jülich, 2000: pp 507−540.
(91) Jensen, F. *J. Chem. Phys.* **2001**, *115*, 9113–9125.
(92) Jensen, F. *J. Chem. Phys.* **2002**, *116*, 3502.
(93) Jensen, F. *J. Chem. Phys.* **2002**, *116*, 7372–7379.
(94) Jensen, F. *J. Chem. Phys.* **2002**, *117*, 9234–9240.
(95) Jensen, F. *J. Chem. Phys.* **2003**, *118*, 2459–2463.
(96) Jensen, F.; Helgaker, T. *J. Chem. Phys.* **2004**, *121*, 3463–3470.
(97) Martin, J. M. L.; Sundermann, A. *J. Chem. Phys.* **2001**, *114*, 3408–3420.
(98) Dunlap, B. I. *J. Mol. Struct.* (*THEOCHEM*) **2000**, *529*, 37–40.
(99) Reed, A. E.; Curtiss, L. A.; Weinhold, F. *Chem. Rev.* **1988**, *88*, 899–926.